RESEARCH ARTICLE

Optimization of electric field treatment parameters for tomato seeds based on an improved AO-ENN model

Jianzhong Chen[1], Jianfang Hu[1], Zhiwei Li[2], Huiling Du[3, *]

[1]Department of Agriculture and Forestry and Engineering, Shanxi Yuncheng Vocational and Technical College of Agriculture, Yuncheng, Shanxi, China. [2]College of Information Science and Engineering, [3]Shanxi Institute of Functional Agriculture, Shanxi Agricultural University, Taigu, Shanxi, China.

Received: March 25, 2026; **accepted:** July 16, 2026.

Tomato is a globally important economic crop, and the germination quality of its seed directly affects seedling establishment and final yield. Electric field treatment (EFT) has been shown to regulate seed physiological metabolism, but its effects depend on the synergistic optimization of multiple parameters such as field strength, treatment time, and pulse frequency, which exhibit complex nonlinear interactions. Existing single-factor or empirical methods cannot achieve global co-optimization. This study addressed the challenge of multi-parameter co-optimization in the process of EFT of tomato seeds using the improved Aquila optimizer algorithm and Elman neural network model. The algorithm's performance was enhanced by introducing a nonlinear convergence factor, adaptive Cauchy mutation, and elite back-learning strategies. Furthermore, a nonlinear mapping model between electric field parameters and seed germination and physiological indicators was established using the dynamic memory characteristics of the Elman neural network. This model demonstrated significantly higher prediction accuracy than the control model of BP neural network and PSO-ENN, and the optimal treatment parameters were found to be 3.5 kV/cm electric field strength, 120 s treatment time, and 15 Hz pulse frequency. Validation experiments showed that, under these conditions, the tomato seed germination rate and α-amylase activity reached 93.8% and 31.6 U/g, which were 19.1% and 43.7% higher than that in the control group, respectively. The seedling dry weight increased by 29.3%, significantly improving photosynthetic performance. The study confirmed a significant interaction between electric field strength, time, and frequency, requiring co-optimization. This research provided a precise and efficient intelligent optimization method for EFT of seeds, contributing to the standardized application of physical agriculture.

Keywords: electric field treatment; tomato seeds; parameter optimization; aquila optimizer; Elman neural network; germination rate; physiological indicators.

[*]**Corresponding author:** Huiling Du, Shanxi Institute of Functional Agriculture, Shanxi Agricultural University, Taigu, Shanxi 030800, China. Email: duhuiling66@163.com.

Introduction

Tomato (*Solanum lycopersicum* L.) is one of the most widely cultivated and economically important vegetable crops globally, and the germination quality of tomato seeds directly determines seedling establishment, growth uniformity, and final yield [1, 2]. Electric field treatment (EFT) has emerged as a promising physical technology for seed improvement. Through mechanisms such as dielectrophoresis, cell membrane electroporation, and regulation of enzyme activities, EFT can significantly enhance the physiological state of seeds, increase the activity of key germination enzymes like α-amylase, accelerate the conversion of storage substances, and provide energy for germination [3, 4].

Recent studies have explored various physical and physicochemical methods to improve seed performance. Yagız *et al*. treated tomato seeds with TiO_2 nano-priming to improve production efficiency, achieving significantly higher germination rates and seedling growth [5]. Ussenov *et al*. investigated the effects of non-thermal plasma treatment on wheat seeds and found optimized germination parameters and increased α-amylase activity [6]. Veerana *et al*. reviewed the broad application prospects of non-thermal plasma technology in sustainable agriculture [7]. Azrial *et al*. studied the differential effects of extremely low-frequency magnetic fields on old rice seeds, showing that exposure time differentially affected seed vigor [8]. Zhang *et al*. summarized recent progress in pulsed electric field technology for fresh food preservation, indicating its significant potential in maintaining quality [9]. Despite its great potential, the practical application of EFT is highly dependent on the complex and synergistic interaction among multiple parameters such as electric field strength (EFS), treatment time, and pulse frequency [10, 11]. These parameters have significant nonlinear interaction effects, making global parameter optimization a typical multi-dimensional and nonlinear problem, and traditional single-factor or empirical optimization methods cannot achieve global co-optimization.

This study developed an intelligent optimization method that combined an improved Aquila optimizer (AO) algorithm with an Elman neural network (ENN) to establish a high-precision prediction model for the relationship between electric field parameters and seed germination and physiological indicators and determined the optimal EFT parameters for tomato seeds. The standard AO algorithm was improved by introducing a nonlinear convergence factor, adaptive Cauchy mutation, and elite back-learning strategies to enhance convergence speed and escape from local optima. The improved AO was then integrated with ENN, which possessed dynamic memory characteristics suitable for capturing the cumulative effects of EFT, constructing a nonlinear mapping model between electric field parameters (EFP) (EFS, time, frequency) and seed germination indicators (germination rate, α-amylase activity, *etc*.). This research provided a precise and efficient intelligent optimization method for seeds' EFT, overcoming the limitations of empirical and single factor approaches, confirmed the significant interaction among EFS, time, and frequency, highlighting the necessity of co-optimization, and contributed to the standardized application of physical agriculture while offering a transferable framework for optimizing other seed treatment processes.

Materials and methods

EFP model construction based on ENN

An EFP model was proposed to optimize EFT parameters and improve the effect of EFT on tomato seeds based on ENN. ENN has strong nonlinear mapping ability and dynamic characteristics and is suitable for handling the complex relationship between EFPs and germination rate [15, 16]. The ENN model constructed by using TensorFlow (https://www.tensorflow.org/) contained a four-layer structure including the input layer receiving three EFPs (EFS, processing time, and pulse frequency), the hidden layer (HL) performing nonlinear transformation to explore the potential correlation between the parameters and germination indices, the receiving layer remembering the previous moment's output state, giving the network dynamic characteristics, and enabling it to adapt more effectively to temporal changes in parameters during electric field processing, and the output layer predicting the germination indices of tomato seeds including germination rate, germination index, α-amylase activity, and soluble sugar content. This structure enabled the ENN to establish a relatively accurate relationship model between EFPs and multidimensional germination indices, laying the foundation for subsequent parameter optimization [17, 18]. The network input vector was composed of normalized EFPs as below.

$$X(t) = [E(t), T(t), F(t)]^T \quad (1)$$

where $E(t)$ was the EFS at time t. $T(t)$ was the processing time. $F(t)$ was the pulse frequency. T was transpose. The activation state of the HL at time t was determined by the current input and the context layer state as follows.

$$H(t) = f_h(W_{ih} \cdot X(t) + W_{ch} \cdot C(t-1) + b_h) \quad (2)$$

where $H(t)$ was the activation state of the HL at time t. $X(t)$ was the current input. $C(t-1)$ was the state of the context layer at the previous time step. W_{ih} was the weight matrix from the input layer to the HL. W_{ch} was the weight matrix from the context layer to the HL. b_h was the bias vector of HL. f_h was the activation function of HL. The hyperbolic tangent function was selected in this study to enhance the nonlinear expressive power. The context layer was the ENN's dynamic memory unit, and its state directly copied HL's output from the previous time step as follows.

$$C(t) = H(t-1) \quad (3)$$

The output layer received the output of the HL and generated the final prediction value as below.

$$Y(t) = f_o(W_{ho} \cdot H(t) + b_o) \quad (4)$$

where W_{ho} was the weight matrix from the HL to the output layer. b_o was the bias vector of the output layer. f_o was the activation function of the output layer. $Y(t)$ was the seed physiological index vector predicted by the model. To train the network, a loss function was defined to measure the difference between the predicted and actual observations. The mean squared error was utilized as the loss function as follows.

$$L(\theta) = \frac{1}{N}\sum_{t=1}^{N} ||D(t) - Y(t)||^2 \quad (5)$$

where $Y(t)$ was the predicted value. $D(t)$ was the actual observed value. N was the number of samples in a training batch. θ was the set of all trainable parameters in the network. The expansion of the ENN in the time dimension revealed its process of handling sequence data. Specifically, the ENN constructed a dynamic recursive structure by storing the output of the HL at the previous time step in the receiving layer and feeding it back to the HL as additional input at the next step. This characteristic enabled it to capture the cumulative effect of electric field parameters changing over time such as the short-term effect of the initial EFS on seed epidermal permeability and the long-term effect of pulse frequency on enzyme activity regulation in the later stage. Due to the existence of recursive connections, the ENN was trained using a backpropagation algorithm with time truncation. The update gradient of its parameter was determined by the cumulative error of multiple time steps as follows.

$$\Delta\theta = -\eta \sum_{k=0}^{\tau} \frac{\partial L(t-k)}{\partial \theta} \quad (6)$$

where η was the learning rate. τ was the backtracking time step. $\partial L(t-k)$ was the partial derivative of the loss function L with respect to the model parameter θ at time $t-k$. t was the index of the current time step. k was the loop variable in the summation operation. Through the above model construction, the mapping relationship between EFPs based on ENN and tomato seed germination indices was established. The model captured the temporal dynamic characteristics during the electric field processing through a transition layer, thus more comprehensively reflecting the combined influence of EFPs on seed germination.

EFP model optimization based on improved AO-ENN

While optimizing EFPs using a single ENN model can capture the complex relationship between EFPs and seed germination indices, it still suffers from local optima and slow convergence. This study used an enhanced AO algorithm to optimize the ENN by proposing an AO-ENN EFP model, which encoded the weights and thresholds of the ENN as individual positions within the improved AO algorithm, iteratively updating to find the optimal combination of weights and thresholds to minimize the prediction error of the ENN. The AO-ENN ensemble model used ENN as the core prediction unit and the AO algorithm to globally optimize its weights and thresholds. The connection weights and neuron thresholds of each layer of ENN were encoded into individual position vectors in the AO algorithm with everyone representing a potential combination of ENN parameters. During iteration, the AO algorithm simulated the hunting strategy of an eagle flock, dynamically adjusting the search direction. It first used global search to locate the advantageous region and then a local development strategy to finely search for the optimal solution, effectively balancing exploration and development capabilities [19, 20]. The study constructed all trainable parameters in ENN into a high-dimensional vector and defined it as a function optimization problem in high-dimensional space as below.

$$\theta^* = \arg\min_\theta \mathrm{F}\ (\theta) = \arg\min_\theta \left(RMSE_{val}(\theta) \right) \tag{7}$$

where $\mathrm{F}(\theta)$ was the objective function. $RMSE_{val}$ was the root mean square error of the model on the validation set. This definition transformed the problem of finding the optimal neural network parameters into a clear and computable optimization objective, providing a direct basis for introducing the AO algorithm. The standard AO algorithm performed global exploration by simulating a high-altitude eagle patrol to find prey areas. The corresponding position update strategy for this behavior was shown below.

$$X_1(t+1) = X_{best}(t) \times (1 - \tfrac{t}{T}) + (X_M(t) - X_{best}(t) \cdot rand) \tag{8}$$

where $X_{best}(t)$ was the current optimal individual position. $X_M(t)$ was the population average position. T was the maximum number of Epochs. $rand \in [0,1]$. While the strategy by combining the optimal solution with population average information could guide individuals to explore a wide space, its linearly decaying exploration weight $(1 - \frac{t}{T})$ lacked flexibility when dealing with complex error surfaces. Therefore, this study improved the AO algorithm. Each individual eagle represented a candidate set of ENN parameters. Let the population size be M, then the position vector X_i of the i -th individual directly encoded the parameter vector as below.

$$X_i = (x_{i1}, x_{i2}, ..., x_{iD}), LB_d \le x_{id} \le UB_d \tag{9}$$

where LB_d and UB_d defined the search boundary of the d-th dimension parameter. For dynamic equilibrium exploration and development, the linear term in the standard strategy was replaced with a nonlinear adaptive convergence factor $CF(t)$ as follows.

$$CF(t) = CF_{\max} \times \left(\frac{CF_{\min}}{CF_{\max}} \right)^{\left(\frac{t}{T}\right)^\lambda} \tag{10}$$

where $CF_{\max} = 1$, $CF_{\min} = 0.2$, and $\lambda = 1.5$. The improved AO exploration strategy was shown below.

$$X_1(t+1) = X_{best}(t) \times CF(t) + (X_M(t) - X_{best}(t) \cdot rand) \tag{11}$$

Among them, the factor $CF(t)$ decreased slowly in the early stage of iteration to maintain strong exploration ability, while it decreased rapidly in the later stage to promote rapid convergence. To determine whether the algorithm got stuck in a local optimum, the population diversity $Div(t)$ during iteration was defined as follows.

$$Div(t) = \frac{1}{M} \sqrt{\sum_{i=1}^{M} \sum_{d=1}^{D} (x_{id}(t) - \overline{x}_{id}(t))^2} \tag{12}$$

where $\overline{x}_{id}(t)$ was the average value of the population in the d -th dimension. D was the dimension of the problem. $\overline{x}_{id}(t)$ was the component value of the population in the d -th dimension. When the triggering condition was met, mutation was applied to the global optimal solution to escape the local optimum as below.

$$\begin{cases} X'_{best}(t) = X_{best}(t) + X_{best}(t) \otimes Cauchy(z, \sigma(t)^2) \\ \sigma(t) = \sigma_{\max} - (\sigma_{\max} - \sigma_{\min}) \times \dfrac{t}{T} \end{cases} \quad (13)$$

where $X'_{best}(t)$ was the new candidate solution generated after Cauchy mutation in the t-th iteration. $Cauchy(0, \sigma(t)^2)$ was a random vector, each component of which was a random number independently following a Cauchy distribution. $\sigma(t)^2$ was the scale parameter. z was the position parameter. $\sigma_{\max}$ was the max value of the scale parameter. $\sigma_{\min}$ was the mini value of the scale parameter. To further improve search efficiency, the study generated the reverse solution X^o_{elite} for contemporary elite individuals X_{elite} to explore potential better regions as follows.

$$X^o_{elite,d}(t) = s \cdot (LB_d + UB_d) - X_{elite,d}(t) \quad (14)$$

where $s \in (0, 1)$ was a random number. The improved AO algorithm enhanced performance mainly through three strategies. Strategy 1 replaced the standard linear factor with a nonlinear adaptive convergence factor, initially slowing down to enhance global exploration, and later rapidly slowing down to focus on local development, achieving dynamic equilibrium in the search. Strategy 2 applied Cauchy distribution perturbation to the optimal solution when population diversity was insufficient, utilizing its long-tail characteristic to generate large jumps to escape local optima. Strategy 3 generated reverse solutions for elite individuals and updated them selectively. These three strategies worked together to enhance the algorithm's ability to optimize globally and converge accurately in complex parameter spaces. The core objective of the improved algorithm was to minimize the prediction error by optimizing the ENN parameters. The fitness function was expressed as the reciprocal of the validation set error as follows.

$$Fitness(Xi) = \frac{1}{RMSE_{eval}(\theta(X_i)) + \epsilon} = \frac{1}{\sqrt{\frac{1}{N_v}\sum_{j=1}^{N_v}\sum_{l=1}^{4}(d_{jl} - y_{jl}(\theta(X_i)))^2 + \epsilon}} \quad (15)$$

where *Fitness*(X_i) was for the fitness value of the i -th individual X_i in the Aquila population. $\theta(X_i)$ was the ENN parameters obtained by decoding the individual's position. N_v was the number of validation samples. d_{jl} and y_{jl} were the true and predicted values of the l -th index of the j -th sample, respectively. ϵ was a small constant to prevent division by zero. The operation flow of the EFP model based on the improved AO-ENN began with the initialization and encoding phase. The dataset of EFPs and physiological indicators was divided into training and validation sets, and an ENN structure was defined to encode the position vectors of individual eagles into ENN parameters. The core part was the iterative search loop of the improved eagle optimization algorithm. The population was first initialized. Each individual passed through the "fitness evaluation" module, where its position was decoded into ENN parameters and its fitness was calculated on the validation set. The "improved position update" was then performed, employing four hunting strategies combined with a nonlinear convergence factor. In the "improved strategy application" stage, population diversity was continuously monitored. If it was too low, adaptive Cauchy mutation was triggered, and back-learning was performed on elite individuals to expand the search range. After the termination condition was met, the process entered the output and application phase. The globally optimal position was output and decoded into the optimal ENN parameters.

Plant seed treatment and germination

The domestic greenhouse variety "Jinpeng" tomato seeds were obtained from the Institute of Vegetables and Flowers, Chinese Academy of Agricultural Sciences, Beijing, China. The seeds had a purity ≥ 98%, germination rate ≥ 90%, and moisture content ≤ 8%. Before the experiment, seeds were placed in a constant temperature and humidity chamber with 25 ± 1°C and 45% relative humidity for 7 days to balance moisture and uniformize their initial physiological state. The EFT system included a DW-P303-1AC high-voltage electrostatic generator (Beijing Dongfang Walker Technology Co., Ltd., Beijing, China) with output voltage of 0 – 100 kV and accuracy ±0.5%, a parallel 30 cm diameter circular stainless steel plate electrode device with electrode spacing adjustable from 1 – 10 cm, a pulse modulation module with frequency range of 1 – 100 Hz and duty cycle of 10 – 90%, and a LabVIEW-based intelligent control system (National Instruments, Austin, TX, USA). A three-factor, five-level quadratic regression orthogonal design was employed to investigate the effects of EFS (1 - 5 kV/cm), treatment time (60 - 300 s), and pulse frequency (5 - 25 Hz) on tomato seed germination. The experiment consisted of 20 groups including 8 cubic points, 6 axial points, and 6 center points with 6 repeats to assess error. Each group treated 300 seeds with 3 replicates. Seeds were evenly placed between parallel plate electrodes during treatment to ensure consistent electric field conditions. After treatment, tomato seeds were placed in a standard germination box with diameter of 12 cm and height of 5 cm with double-layered filter paper as the germination bed. 8 mL of distilled water was added for humidification. Germination was carried out in a constant temperature incubator at 25 ± 1°C and 75% relative humidity in darkness with daily watering to maintain moisture. The germination experiment lasted for 10 days with daily recording of germinated seeds. Germination potential (day 3), germination rate (day 7), germination index, and vigor index were calculated according to international standards. The collected data were split into training set (70%), validation set (15%), and test set (15%) for model training and evaluation.

Determination of enzyme activities

The α-amylase and dehydrogenase activities of germinated seeds were determined on days 3 and 7. α-amylase activity was determined by using α-Amylase Activity Assay Kit (Sigma-Aldrich, St. Louis, MO, USA) following manufacturer's instructions. Dehydrogenase activity was determined by triphenyltetrazolium chloride (TTC) reduction method. A standard curve was obtained using a series of TTC (Sigma-Aldrich, St. Louis, MO, USA) standard solutions. Approximately 0.2 g of fresh seed tissue was weighed, washed with distilled water, and blotted dry with filter paper. The sample was placed in a centrifuge tube containing 1 mL of TTC assay buffer prepared by mixing 0.4% (w/v) TTC in 0.05 M phosphate buffer at pH 7.0 and incubated at 37°C in darkness for 3 h. The reaction was terminated by adding 1 mL of 1 mol/L sulfuric acid and immediately cooled on ice for 5 min. The tissue was then blotted dry and grounded thoroughly with 1 mL of ethyl acetate to extract the red formazan product (triphenylformazone) (TF). The homogenate was transferred to a centrifuge tube and brought to a final volume of 2 mL by ethyl acetate. After centrifugation at 10,000 g for 5 min at 4 °C, the absorbance of the supernatant was measured at 485 nm using a Shimadzu UV-1800 spectrophotometer (Shimadzu, Kyoto, Japan) with ethyl acetate as the blank. The enzyme activity was expressed as mg TTC reduced per gram of seed per hour (mg TTC/g·h).

Measurement of soluble sugar content

Soluble sugar contents on days 3 and 7 were determined by the anthrone colorimetric method. The anthrone reagent (Sigma-Aldrich, St. Louis, MO, USA) was freshly prepared at a concentration of 2 g/L in 80% (v/v) sulfuric acid. A standard curve was constructed using glucose (Sinopharm Chemical Reagent Co., Ltd., Shanghai, China) standard solutions in the ranges of 10 to 200 μg/mL. Approximately 0.1 g of fresh seed tissue was homogenized in 5 mL of distilled water, and the homogenate was placed in a boiling water bath for 10 min to extract soluble sugars before cooling down to room temperature and centrifuging at 3,000 g for 15 min to collect supernatant. 0.2 mL of the supernatant was mixed with 1 mL of freshly prepared anthrone reagent and placed in a boiling water bath for 7 min for color development. The reaction was then terminated by cooling in ice water for 25 min. The absorbance was measured at 620 nm using spectrophotometer. The soluble sugar content was expressed as glucose equivalents in mg/g fresh weight.

Comparison models and implementation

The improved AO-ENN model was compared with standard backpropagation neural network (BPNN) and particle swarm optimization-Elman neural network (PSO-ENN) models using the same training, validation, and test datasets and the same network structure. BPNN was implemented using the neural network toolbox of MATLAB (https://www.mathworks.com/products/neural-network.html) with default parameters of training function of Levenberg-Marquardt, learning rate of 0.01, number of hidden neurons of 10. PSO-ENN model combined a standard PSO algorithm with ENN. The PSO algorithm was implemented in Python (version 3.8) using the pyswarm library (https://pythonhosted.org/pyswarm/). The PSO parameters were set as swarm size of 30, inertia weight of 0.7, cognitive and social coefficients of 1.5 each, and maximum Epochs of 200.

EFP optimization experiment

Based on the improved AO-ENN model, a grid search method was used for multi-objective optimization to maximize germination rate and α-amylase activity. A multi-objective optimization function was established to determine the optimal EFT parameters. Multiple control experiments were conducted near the optimal parameter points to verify the results. A total of six treatment groups were tested as optimized group (OG) with AO-ENN recommended parameters of EFS 3.5 kV/cm, 120 s, 15 Hz; high-intensity short-time group (HST) with EFS 5.0 kV/cm, 60 s, 15 Hz; low-intensity long-time group (LLT) with EFS 1.0 kV/cm, 300 s, 15 Hz; high-frequency deviation group (HFD) with EFS 3.5 kV/cm, 120 s, 25 Hz; low-frequency deviation group (LFD) with EFS 3.5 kV/cm, 120 s, 5 Hz; and control group (CG) with no EFT.

Physiological and biochemical indicators and seedling growth characteristics

To explore the sustained effects of EFT on tomato seed germination and subsequent growth, the dynamic changes of key physiological and biochemical indicators during seed germination under the optimized parameter treatment (3.5 kV/cm, 120 s, 15 Hz) were systematically measured, and the growth performance of seedlings was tracked and observed. For seed germination and physiological status, the germination rate (%) on day 7, germination potential (%) on day 3, germination index, vigor index, α-amylase activity (U/g fresh weight), dehydrogenase activity (mg TTC reduced/g·h), and soluble sugar content (mg/g fresh weight, glucose equivalents) were determined. For seedling growth characteristics, the plant height (cm), stem diameter (mm), root length (cm), total fresh weight per seedling (g), total dry weight per seedling (g), root-to-shoot ratio, chlorophyll SPAD value, net photosynthetic rate (μmol CO_2/m²·s), and stomatal conductance (mol H_2O/m²·s) were measured 21 days after sowing. All measurements were performed in triplicate for each treatment group (optimized group *vs*. control group). Seedling growth parameters were measured using standard agronomic methods with plant height from the cotyledon node to the apical meristem, stem diameter at the cotyledon node using a digital caliper, and root length as the longest primary root. Fresh weight was recorded immediately after harvesting, and dry weight was measured after drying at 70°C to constant weight (approximately 48 h). Chlorophyll content (SPAD value) was measured using Konica SPAD-502Plus portable chlorophyll meter (Konica Minolta, Tokyo, Japan) on the first fully expanded leaf. Net photosynthetic rate and stomatal conductance were measured using LI-COR LI-6400XT portable photosynthesis system (LI-COR Biosciences, Lincoln, NE, USA) under controlled light intensity of 1,000 μmol/m²·s and ambient CO_2

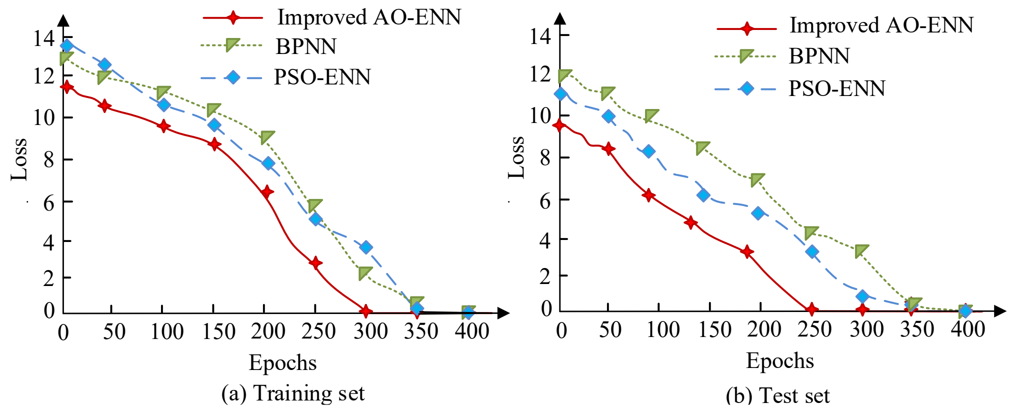

Figure 1. Comparison of training loss values of different models in training and test sets.

concentration of 400 μmol/mol between 9:00 am and 11:00 am.

Statistical analysis

All the results were expressed as mean ± standard deviation (SD). SPSS (version 26.0) (IBM, Armonk, NY, USA) was employed for statistical analysis. Differences among multiple treatment groups (OG, HST, LLT, HFD, LFD, and CG) were assessed using one-way analysis of variance (ANOVA) followed by Tukey's honest significant difference (HSD) post hoc test. For comparisons between the optimized group (OG) and the control group (CG) for seedling growth characteristics and physiological indicators, an independent-samples Student's t-test was applied. *P* value less than 0.05 was considered as statistically significant, while *P* value less than 0.01 was considered highly significant.

Results and discussion

Model performance evaluation

The performance comparison of different models showed that, on the training set, the improved AO-ENN had an initial loss of 11.6, which approached zero after 300 epochs, while the initial losses of BPNN and PSO-ENN were 13.1 and 13.8, respectively, both requiring 400 Epochs to converge to 0 (Figure 1a). On the test set, the initial loss of improved AO-ENN was 9.7, which approached 0 after 250 Epochs, while the initial losses of BPNN and PSO-ENN were 12.2 and 11.3, respectively, requiring 350 and 400 Epochs to converge to 0 (Figure 1b). The results indicated that, with the same number of training Epochs, improved AO-ENN had significantly lower losses on both the training and test sets than the other two models and converged faster. The comparison of the analytical accuracy of different methods showed that, in the training dataset, the improved AO-ENN achieved an accuracy of 98.4% after 250 Epochs, higher than BPNN (83.9%) and PSO-ENN (83.2%) (Figure 2a). In the test dataset, the improved AO-ENN also performed best, achieving an accuracy of 97.4% after 250 Epochs, better than PSO-ENN (83.8%) and BPNN (83.6%) (Figure 2b). The results indicated that the improved AO-ENN model had higher analytical accuracy.

EFP optimization

Based on the improved AO-ENN model and the experimental results, the optimal treatment parameters were determined as 3.5 kV/cm of EFS, 120 s of treatment time, and 15 Hz of pulse frequency. The results for the six treatment groups showed that, compared to CG, OG achieved the highest germination rate of 93.8 ± 1.2% and α-amylase activity of 31.6 ± 1.5 U/g ($P < 0.01$). HFD group also showed significantly improved germination rate of 91.6 ± 1.4% and α-amylase activity of 29.2 ± 1.3 U/g ($P < 0.01$), while LFD group yielded germination rate of 89.3 ± 1.6% and α-amylase

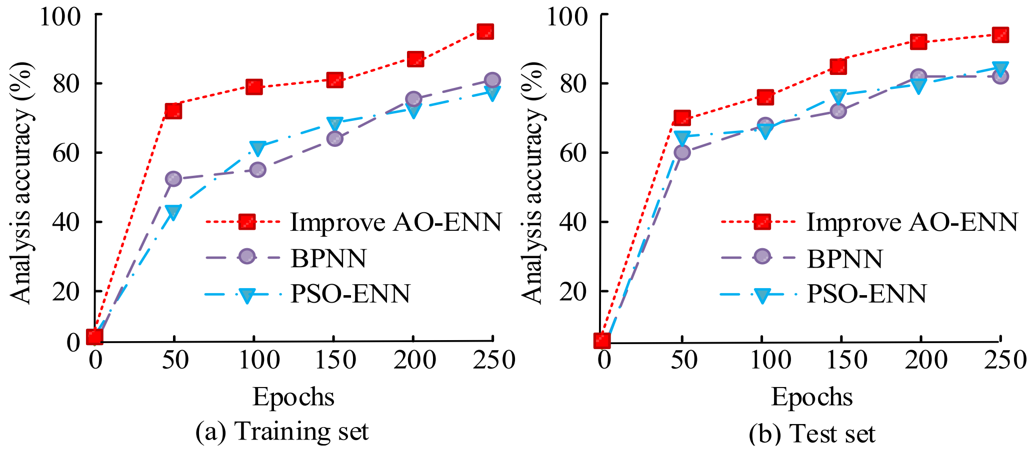

Figure 2. Comparison of analysis accuracy of different models in training and test sets.

Table 1. Germination and physiological responses of tomato seeds under different EFP combinations.

Treatment group	Electric field strength (kV/cm)	Treatment time (s)	Pulse frequency (Hz)	Germination rate (%)	α-amylase activity (U/g)	*P* value
CG	0	0	0	74.7 ± 2.3	22.0 ± 1.2	–
OG	3.5	120	15	93.8 ± 1.2	31.6 ± 1.5	<0.01
HST	4.5	60	15	85.2 ± 1.8	26.5 ± 1.3	<0.05
LLT	2.5	180	15	88.4 ± 1.5	26.3 ± 1.2	<0.05
HFD	3.5	120	25	91.6 ± 1.4	29.2 ± 1.3	<0.01
LFD	3.5	120	5	89.3 ± 1.6	27.8 ± 1.4	<0.01

activity of 27.8 ± 1.4 U/g ($P < 0.01$). HST and LLT groups both exhibited moderate improvements with germination rates of 85.2 ± 1.8% and 88.4 ± 1.5% and α-amylase activities of 26.5 ± 1.3 U/g and 26.3 ± 1.2 U/g, respectively ($P < 0.05$) (Table 1). These results demonstrated that the AO-ENN optimized parameters produced the best overall effects, and both upward and downward deviations from the optimal frequency or intensity reduced germination performance. The comparison of different EFT schemes showed that the comprehensive evaluation value of 0.902 of the improved AO-ENN was higher than that of the other groups (Figure 3a). Improved AO-ENN had the highest soluble sugar content (12.4) (Figure 3b) and the highest germination index of 52.4 (Figure 3c), comprehensively leading other treatment groups and the control group. The findings demonstrated that the EFPs optimized by the model could simultaneously and significantly improve seed germination vigor, energy metabolism, and overall benefits, and the effect was better than any single parameter empirical scheme.

Validation of physiological and biochemical indicators and analysis of seedling growth characteristics

The effects of optimized EFT on tomato seedling growth characteristics 21 days after sowing showed that all growth and physiological indicators in the EFT group were greatly better than those in the control group. Plant height, stem diameter, and root length increased by 22.2%, 21.9%, and 25.4%, respectively. The total fresh weight and total dry weight increased by 28.6% and 29.3%, respectively. The root-to-shoot ratio (root dry weight/shoot dry weight) increased slightly but not significantly, indicating that the electric field promoted a relatively balanced effect on both the aboveground and

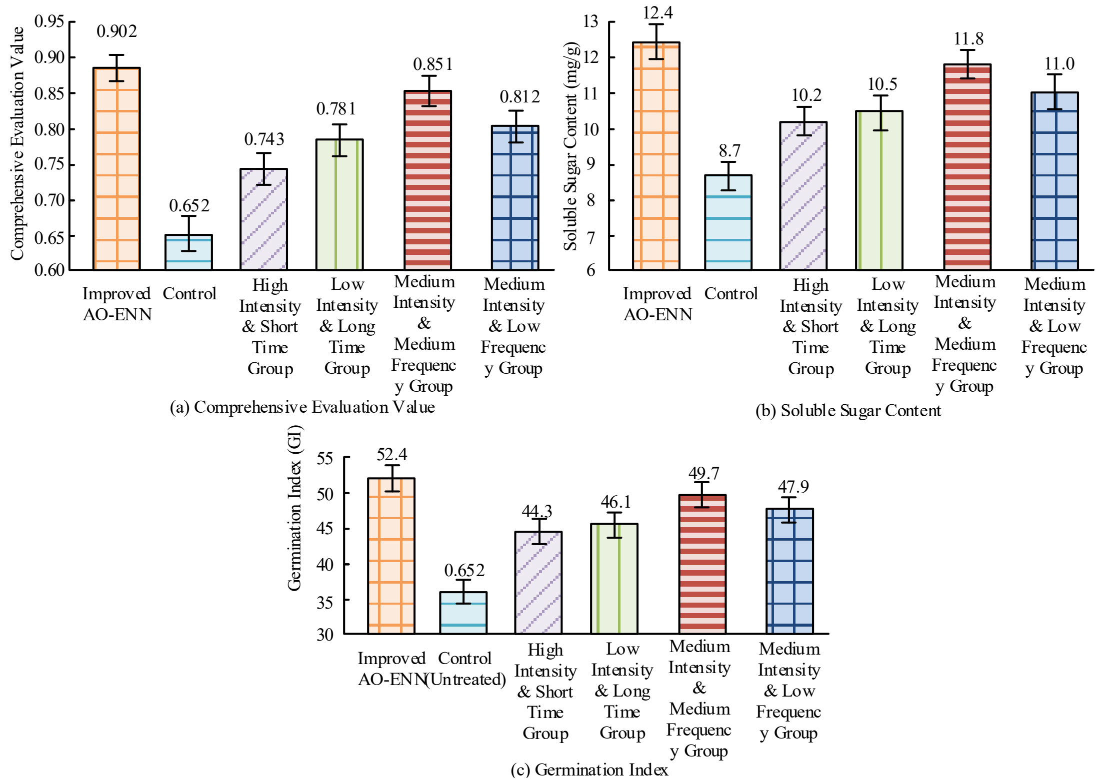

Figure 3. Performance comparison of different electric field treatment schemes.

Table 2. Effects of electric field treatment on growth characteristics of tomato seedlings 21 days after sowing.

Growth and physiological indicators	Control group	Electric field treatment group (3.5 kV/cm, 120 s, 15 Hz)	Increase rate (%)	*P* value
Plant height (cm)	15.3 ± 1.2	18.7 ± 1.4	+22.2	< 0.01
Stem diameter (mm)	3.2 ± 0.3	3.9 ± 0.4	+21.9	< 0.01
Root length (cm)	12.6 ± 1.1	15.8 ± 1.3	+25.4	< 0.01
Total fresh weight (g/plant)	2.8 ± 0.3	3.6 ± 0.4	+28.6	< 0.01
Total dry weight (g/plant)	0.41 ± 0.05	0.53 ± 0.06	+29.3	< 0.01
Root-shoot ratio	0.30 ± 0.03	0.32 ± 0.04	+6.7	0.15
Chlorophyll SPAD value	32.4 ± 2.1	38.7 ± 2.4	+19.4	< 0.01
Net photosynthetic rate (μmol/m^2·s)	8.7 ± 0.7	11.2 ± 0.9	+28.7	< 0.01
Stomatal conductance (mmol/m^2·s)	0.21 ± 0.03	0.28 ± 0.04	+33.3	< 0.01

Note: Data were presented as mean ± SD (n=3). *P* values were the comparison of the electric field treatment group with the control group.

underground parts. Physiologically, chlorophyll SPAD value, net photosynthetic rate, and stomatal conductance increased by 19.4%, 28.7%, and 33.3%, respectively, indicating that the electric field effectively enhanced the photosynthetic capacity and gas exchange efficiency of tomato seedlings (Table 2). EFT significantly improved tomato seed germination performance and continuously promoted seedling growth, providing a basis for the agricultural application of this technology. The dynamic changes of relevant physiological indicators demonstrated that the α-amylase activity in the electric field treated group was greatly higher than that in the control group throughout the germination cycle with the

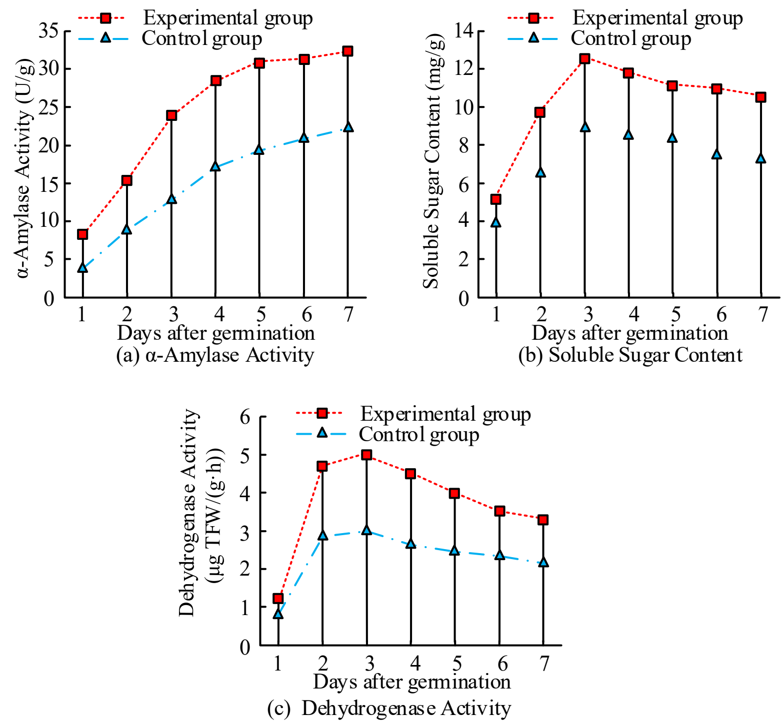

Figure 4. Effects of dynamic changes of key physiological indicators on tomato seed germination.

difference widening rapidly from day 2 onwards, indicating that EFT significantly promoted starch decomposition (Figure 4a). The soluble sugar content in the treated group reached its peak on day 3 as 12.5 mg/g, greatly higher than the peak of 8.8 mg/g in the control group, providing more energy and osmotic regulators for early germination (Figure 4b). The dehydrogenase activity in the treated group began to rise on day 2 as 4.8 μg TFW/(g·h) with an earlier peak and a much higher intensity than the control group, indicating a significant enhancement in respiratory metabolism (Figure 4c). EFT not only increased the intensity of seed metabolism but also advanced the metabolic peak, explaining the higher germination potential and more uniform germination from a physiological perspective.

Conclusion

This study successfully developed an improved AO-ENN optimization model to address the multi parameter co-optimization problem in EFT of tomato seeds. The model demonstrated superior prediction accuracy and convergence speed compared to conventional BPNN and PSO-ENN models. The optimized electric field parameters significantly enhanced seed germination and seedling growth, confirming the synergistic interaction among EFS, treatment time, and pulse frequency. Physiological analyses revealed that the optimized treatment promoted key metabolic enzyme activities and advanced the metabolic peak during germination. This research provided an intelligent, high precision method for physical seed treatment, contributing to the standardized application of physical agriculture. Future work should extend the model to other crop varieties and incorporate additional physiological indicators to improve generalizability.

Acknowledgements

This research was supported by Central Guided Local Science and Technology Development Fund

Project (Grant No. YDZJSX20231A042), National Key Research and Development Program Project (Grant No. 2017YFD0701501), Shanxi Province Agricultural Science and Technology Research and Development Project (Grant No. 2013031101).

References

1. Yang G, Xu J, Xu Y, Guan X, Ramaswamy HS, Lyng JG, *et al*. 2024. Recent developments in applications of physical fields for microbial decontamination and enhancing nutritional properties of germinated edible seeds and sprouts: A review. Crit Rev Food Sci Nutr. 64(33):12638-12669.
2. Rana S, Kapoor S, Bala M, Surasani VKR, Agarwal A, Thakur M. 2025. Optimization and characterization of tomato seed protein isolate: A sustainable source of functional protein. Biomass Convers Biorefin. 15(9):14339-14356.
3. Wang F, Li L, Li X, Hu X, Zhang B. 2023. Pulsed electric field promotes the growth metabolism of aerobic denitrifying bacteria *Pseudomonas putida* W207-14 by improving cell membrane permeability. Environ Technol. 44(15):2327-2340.
4. Hussein JB, Oke MO, Agboola FF, Oke EO. 2022. Sensitivity analysis and soft-computational prediction of color characteristics of dried tomatoes. Acta Period Technol. 53:285-302.
5. Yagız AK, Çalışkan ME. 2024. Effects of TiO_2 nano-priming on tomato seed germination and plant development. J Anim Plant Sci. 34(1):62-72.
6. Ussenov YA, Akildinova A, Kuanbaevich BA, Serikovna KA, Gabdullin M, Dosbolayev M, *et al*. 2022. The effect of non-thermal atmospheric pressure plasma treatment of wheat seeds on germination parameters and α-amylase enzyme activity. IEEE Trans Plasma Sci. 50(2):330-340.
7. Veerana M, Mumtaz S, Rana JN, Javed R, Panngom K, Ahmed B, *et al*. 2024. Recent advances in non-thermal plasma for seed germination, plant growth, and secondary metabolite synthesis: A promising frontier for sustainable agriculture. Plasma Chem Plasma Process. 44(6):2263-2302.
8. Azrial F, Saputri DA, Listiana I. 2025. The impact of varied exposure duration to ELF (extremely low frequency) magnetic field on old rice (*Oryza sativa* L.) seed viability. J Ilmiah Membangun Desa Pertanian. 10(1):83-97.
9. Zhang Z, Zhang B, Yang R, Zhao W. 2022. Recent developments in the preservation of raw fresh food by pulsed electric field. Food Rev Int. 38(sup1):247-265.
10. Kakarla AK, Akhtar Z, Kim J, Yoon M, Lee D, Choi J. 2025. Beyond the limits of lithium iron phosphate: Cutting edge innovations toward high performance and sustainability for next generation batteries. Interdiscip Mater. 4(6):812-849.
11. Valentine OA, Chukwuebuka AO, Obumneme AE, Solace AA, Ogechi OP, Okwudifele MC, *et al*. 2022. Characterization and treatment of automobile and battery water waste using coagulation and adsorption technique. Traektoriâ Nauki. 8(9):1030-1041.
12. Handa AP, Vian A, Singh HP, Kohli RK, Kaur S, Batish DR. 2024. Effect of 2850 MHz electromagnetic field radiation on the early growth, antioxidant activity, and secondary metabolite profile of red and green cabbage (*Brassica oleracea* L.). Environ Sci Pollut Res. 31(5):7465-7480.
13. Baltacıoğlu C, Yetişen M, Baltacıoğlu H, Karacabey E, Buzrul S. 2024. Impacts of pulsed electric fields (PEF) pre-treatment on the characteristics of fried yellow- and purple-fleshed potatoes: A chemometric-assisted FTIR study. Potato Res. 67(3):1027-1048.
14. Abdel-Baset SH, Eltamany EE, Elhady SS, Abdelrazik E. 2025. Nematocidal activity of white mustard seeds as promising biofumigants for control root-knot nematodes, *Meloidogyne* spp., infecting *Solanum lycopersicum* L. under field conditions. ACS Agric Sci Technol. 5(8):1753-1766.
15. Shelar A, Singh AV, Dietrich P, Maharjan RS, Thissen A, Didwal PN, *et al*. 2022. Emerging cold plasma treatment and machine learning prospects for seed priming: A step towards sustainable food production. RSC Adv. 12(17):10467-10488.
16. Yan B, Li J, Liang QC, Huang Y, Cao SL, Wang LH, *et al*. 2025. From laboratory to industry: The evolution and impact of pulsed electric field technology in food processing. Food Rev Int. 41(2):373-398.
17. Zhang H, Razmjooy N. 2024. Optimal Elman neural network based on improved gorilla troops optimizer for short-term electricity price prediction. J Electr Eng Technol. 19(1):161-175.
18. Dai Y, Wang X, Li Z, He S, Yu B, Zhou X. 2024. Thermal error modeling of electric spindles based on cuckoo algorithm optimized Elman network. Int J Adv Manuf Technol. 132(3):1365-1375.
19. Mutovkina N. 2025. The effectiveness of using fuzzy neural networks in predicting the sales volume of perishable products. Artif Intell Appl. 3(2):203-212.
20. Jacob SL, Habibullah PS. 2025. A systematic analysis and review on intrusion detection systems using machine learning and deep learning algorithms. J Comput Cogn Eng. 4(2):108-120.